Journal of Environmental Management 296 (2021) 113365

Contents lists available at ScienceDirect

Journal of Environmental Management

journal homepage: www.elsevier.com/locate/jenvman

Methylene blue adsorption on thermo plasma expanded graphite in a multilayer column system

Alessio Siciliano [a,*], Giulia Maria Curcio [a], Carlo Limonti [a], Salvatore Masi [b], Michele Greco [b]

[a] Laboratory of Sanitary and Environmental Engineering, Department of Environmental Engineering, University of Calabria, P. Bucci, 87036, Rende, CS, Italy
[b] School of Engineering, University of Basilicata, viale dell'Ateneo Lucano n.10, 85100, Potenza, Italy

ARTICLE INFO

Keywords:
Adsorption kinetics
Adsorption processes
Isotherms
Methylene blue
Thermo plasma expanded graphite

ABSTRACT

The removal of dyes from wastewater is an important topic in environmental applications. Methylene blue (MB) is one of the most worrisome compounds, as it is widespread and used in many industrial activities. Adsorption represents an effective technique for the removal of this contaminant. Thermo plasma expanded graphite (TPEG) is an industrial material characterized by a fibrous morphology, a very low density and overlapped graphene layers. TPEG has a higher specific surface compared to conventional thermo-expanded graphite and it can establish effective attractive forces with charged pollutants. These properties make TPEG a very promising adsorbent material.

In the present work, TPEG was tested in an innovative multilayer column system to treat MB contaminated solutions. Several batch experiments were carried out by varying pH, initial MB concentration and temperature.

The optimal adsorption performance was assessed at pH 11, around which the TPEG assumed the maximum negative charge. Based on these results, the adsorption mechanism appeared to be related mainly to electrostatic interactions. At room temperature, the greatest amount of MB adsorbed on TPEG was detected by treating solutions with an initial concentration of 30 mg_{MB}/L. The temperature increase from 20 to 40 °C caused an enhanced adsorption capacity when concentrations higher than 10 mg_{MB}/L were treated. The adsorption trends were accurately described by a pseudo-second order kinetic law and the adsorption isotherms at 20 and 40 °C were found to follow both the features of Freundlich and Langmuir models. The adsorption capacity was estimated to reach threshold values around 95 mg_{MB}/g_{TPEG} and 265 mg_{MB}/g_{TPEG} at 20 and 40°C, respectively. The Gibbs energy change (ΔG°) was calculated to about −7.80 kJ/mol, which proved that the process is spontaneous from a thermodynamic point of view. Finally, it was verified that TPEG can be efficiently reused 5 times after a simple chemical regeneration phase with HCl.

1. Introduction

Dyes are widely used in various fields, such as textile, constructions, paper, cosmetic, food and leather industries (Rafatullah et al., 2010; Liu et al., 2012, 2018). The possible presence of dyes in the effluents of this kind of activities is a matter of concern, as they may be harmful to both humans and ecosystems (Rafatullah et al., 2010; Yang et al., 2011; Liu et al., 2012, 2018). In particular, some dyes have been found to produce mutagenic and carcinogenic effects on human beings (Aksu, 2005; Liu et al., 2012). Beside this, wastewaters containing dyes are often characterized by high biological and chemical oxygen demands, suspended solids and toxic compounds (Aksu, 2005). However, the main problematic feature of dyes is the coloration that they confer to water, which is recognizable even at low concentrations (Aksu, 2005; Rafatullah et al., 2010). However, the effects on the environment and the dangerousness depend on the chemical compositions, which are very different from one compound to another (Robinson et al., 2001). Indeed, dyes are generally classified in: anionic - direct, acid and reactive dyes; cationic - basic dyes; non-ionic - disperse dyes (Fu and Viraraghavan, 2001; Aksu, 2005).

Methylene blue (MB) is a cationic dye, exploited in several fields, such as for dyeing cotton, wool, silk, paper stock (Rafatullah et al., 2010; Deng et al., 2011; Calimli et al., 2020) and for medical purposes. Although MB is not highly poisonous, it is associated with several diseases. Indeed, the contact with MB causes eye burns, while when ingested it produces nausea, vomiting and diarrhea; furthermore, on

* Corresponding author.
E-mail address: alessio.siciliano@unical.it (A. Siciliano).

https://doi.org/10.1016/j.jenvman.2021.113365
Received 16 April 2021; Received in revised form 9 July 2021; Accepted 20 July 2021
Available online 30 July 2021

inhalation route, it may give rise to dyspnea and tachycardia (Hameed et al., 2007; Rafatullah et al., 2010; Liu et al., 2012). Therefore, the removal of this organic dye is a matter of interest. Indeed, the removal of MB from polluting effluents and contaminated water is mandatory to preserve the quality of water bodies and, therefore, to allow the sustainable management of aquatic resources and to prevent risks for human health.

In the past years, the removal of dyes from industrial wastewater has been tested by exploiting several techniques, which can be reconducted to three main categories: chemical, physical-chemical, and biological processes (Robinson et al., 2001; Forgacs et al., 2004; Singh and Arora, 2011). Chemical treatments include conventional oxidation, advanced oxidation, and electrochemical processes (Singh and Arora, 2011; Tran et al., 2017). Physical treatments are: adsorption, ion exchange, coagulation–flocculation, membrane technology, and irradiation (Singh and Arora, 2011). Biological degradation of dyes involves the use of microorganisms, like bacteria, fungi and yeast, in aerobic or anaerobic conditions (Forgacs et al., 2004; Singh and Arora, 2011).

Among all these methods, adsorption is widely applied, as it is highly effective, cheap and holds relatively low operation costs (Deng et al., 2011; Yang et al., 2011; Liu et al., 2012; Calimli et al., 2020). Furthermore, the adsorption process does not require further reagents and generally shows high removal capacity (Tran et al., 2017). Several materials have been exploited in the adsorption of MB, including activated carbons (Wang et al., 2005; Deng et al., 2009; Dural et al., 2011; Marrakchi et al., 2017), clays (Almeida et al., 2009; Anirudhan and Ramachandran, 2015), silica (Zhao et al., 2008; Peres et al., 2018) and waste materials (Hameed and Ahmad, 2009). Recently, derivatives of graphite such as graphene oxide (GO), have gained great attention in the remediation field due to their high specific surface, excellent electrical and mechanical properties, and good biocompatibility. Indeed, graphene composites have been exploited for the removal of several contaminants: Cr(VI) (Li et al., 2016), Cu^{2+} (Yang et al., 2010), Co(II) (Xing et al., 2016), arsenic (Chandra et al., 2010), phosphorus (Liu et al., 2014), U(VI) (Sun et al., 2014) and various dyes, including methylene blue (Yang et al., 2011; Liu et al., 2012, 2018; Tran et al., 2017, 2020; Calimli et al., 2020). In the adsorption of organic compounds, many kinds of mechanisms (electrostatic interactions, hydrogen bridges, π-π stacking, hydrophobic effects etc.) could play different roles depending on the properties of both chemical species and adsorbent. In the case of graphene oxide, the rich functional groups have a key role in the formation of hydrogen bonds or electrostatic interactions with organic molecules characterized by oxygen and nitrogen functional groups (Wang et al., 2014). Due to the huge localized electron systems, graphene could adsorb the aromatic rings from different organic species by means of strong π-π interactions (Wang et al., 2014). Anyway, hydrogen bonds between the oxygen containing groups of contaminant and graphene could also contribute to the adsorption process (Wang et al., 2014). In recent years, a lot of researches focused on further enhance the material's effectiveness. Many materials derived from graphite, such as graphene supported metals nanoparticles (Khare et al., 2018; Ruan et al., 2018), graphene-based discs (Wang et al., 2013), graphene oxide composites (Fadillah et al., 2019; Wang et al., 2020) have been developed and tested in the removal of different types of contaminants. In this regard, the thermo-plasma expanded graphite (TPEG) represents an interesting option for environmental remediation purposes as an adsorbent material (Caniani et al., 2018; Cuccarese et al., 2021; Pascale et al., 2018). This is an industrial material produced through a first step of chemical intercalation of natural graphite and a second step of very fast expansion conducted by a plasma thermal heating, which ensures an expansion bigger than the typical processes (Cuccarese et al., 2021). TPEG has a fibrous macrostructure characterized by a series of packed graphene layers with presence of mesopores and micropores. The density is extremely low, and the specific surface is higher than conventional graphite derived compounds, such as thermal expanded graphite and graphene oxide (Cuccarese et al., 2021). Moreover, TEPG was found to establish effective electrostatic interactions (Cuccarese et al., 2021), which makes the material particularly suitable in the adsorption of charged compounds. Due to these characteristics, TPEG is a promising adsorbent for the removal of cationic dyes, such as MB. Despite this, the use of TPEG in the removal of pollutants from water and wastewater has been scarcely investigated until now and, to the best of our knowledge, there are no applications for the removal of methylene blue (MB). To overcome this lack of research, in the present study TPEG was applied to treat MB solutions in an innovative multilayer column system. This system overcomes the difficulty in separating the material from the treated solution, which is one of the main technical issues in graphene-type material application. Indeed, column systems with fixed material avoid the solid/liquid separation step which is, instead, necessary in stirred reactors (Mossa Hosseini et al., 2011; Siciliano et al., 2020). Therefore, the risks connected to the loss of adsorbent from the treatment units are prevented. TPEG was placed in the device forming a series of thin layers, separated from each other by permeable membrane discs, in order to avoid packing phenomena which could limit the contact between the solution and the material's surface and, therefore, reduce the adsorbing power.

Several tests were carried out in batch mode to evaluate the effects of pH, initial methylene blue concentration and temperature on the adsorption process. Based on the experimental results, the adsorption kinetics and isotherms were assessed. The reusability of regenerated material was also evaluated.

2. Materials and methods

2.1. Reagents

Thermo-plasma expanded graphite was supplied by Innograf srl (Potenza, Italy). Chemicals of analytical grade were exploited to carry out the adsorption experiments. Methylene blue standard solutions were prepared by using methylene blue trihydrate powder ($C_{16}H_{18}ClN_3S{\cdot}3H_2O$), provided by Alfa Aesar (Kandel, Germany). Hydrochloric acid (37%) and Sodium Hydroxide (1 M), supplied by Carlo Erba (Milan, Italy), were employed for pH adjustment during the tests. All solutions were prepared using double-distilled water.

2.2. Laboratory pilot plant

The experiments were conducted by exploiting a small laboratory pilot plant composed of a multilayer column and auxiliary devices. The column was made in PVC and was characterized by two zones with different dimensions. The upper zone had an internal diameter of 4 cm and a height of about 9 cm (Fig. 1). The zone on the bottom had the internal diameter and the height with dimensions of 4.4 cm and 7 cm, respectively. This compartment was able to house a small cylindrical capsule made in high density polyethylene (HDPE) which was filled with TPEG during the experiments. The internal diameter and height of this box were about 4.2 cm and 2 cm, respectively. The bottom and the cover of the capsule had numerous micro holes, to allow the passage of the water, and the lid was removable. Inside the capsule, the material was divided into 7 thin layers, using six geotextile discs. In addition, two more discs were placed on the top and bottom of the capsule, respectively, to avoid the transport of TPEG flakes with the flow. This system allowed preventing the compaction of the material, which would have led to a less adsorption capacity. To execute the adsorption tests, the capsule, filled with TPEG, was fixed in the proper compartment in the column which was then sealed on the bottom using a watertight cap. This cap had a hole, for the inlet flow. Another hole was made on the upper zone of the column, at a height of 10 cm, for the outlet flow. The auxiliaries of the pilot plant were a beaker placed on a magnetic heating stirrer, a peristaltic pump connected to the column with polypropylene pipes, and pH and temperature bench analysers.

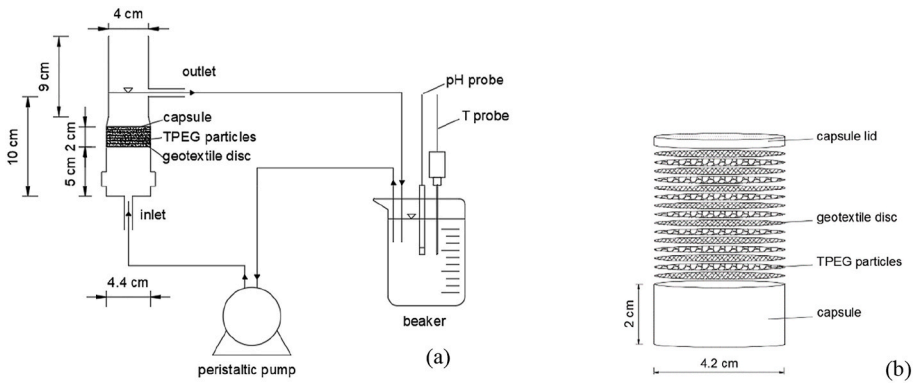

Fig. 1. Scheme of the apparatus exploited during the tests (a) and detail of the capsule which contained TPEG (b).

2.3. Batch adsorption tests

The effects of pH, initial MB concentration (C_i) and temperature (T) on the adsorption process was investigated. Moreover, the adsorption evolution over time was analysed. A first set of experiments was conducted at room temperature (T = 20 ± 2 °C) with pH values of 5, 7, 9, 11 and 13 by treating solutions with an initial concentration of 10 mg_{MB}/L. Once identified the optimal pH, further tests were performed by changing the concentration of MB standard solutions from 2 to 40 mg_{MB}/L. After that, the effect of temperature was investigated through a series of tests conducted at temperatures comprised between 10 ± 2 °C and 60 ± 2 °C, by treating solutions with C_i = 10 mg_{MB}/L. Moreover, at 40 ± 2 °C, the adsorption process was tested by treating solutions with concentrations of 2, 10, 20, 30 and 40 mg_{MB}/L. The tests were performed by using an amount of TPEG comprised between about 0.06 and 0.1 g.

To execute each test, 500 mL of methylene blue standard solution were prepared with the established initial concentration and then the pH was set at the planned value. No further pH corrections were performed during the treatment. To conduct the experiments in batch mode, the prepared MB solution was recirculated from the beaker into the column in up flow mode using a peristaltic pump (Fig. 1). The hydraulic flowrate was set to 250 mL/min which guaranteed a quick recirculation and homogeneity of the MB solution through the column, so that the system behaved like a real batch reactor (Siciliano, 2016; Siciliano and Limonti, 2018). This made it possible to detect the adsorption trends as a function of time. The temperature was held stable by means of the heating plate whose working conditions were controlled by the temperature probe placed inside the beaker. The tests lasted 180 min during which pH and temperature were continuously monitored. To determine the concentration of MB, samples of 10 mL were periodically withdrawn, filtrated and analysed.

The specific adsorbed amount q (mg_{MB}/g_{TPEG}), defined as the amount of MB adsorbed per unit of TPEG mass, was calculated as follows:

$$q = \frac{(C_i - C)\cdot V}{M} \quad (1)$$

where C_i and C (mg_{MB}/L) are, respectively, the concentration of methylene blue at the beginning of the test (initial value) and at a given instant, V (L) is the volume of treated solution and M (g_{TPEG}) is the mass of TPEG used in the experiment.

2.4. Regeneration and reuse of TPEG

A specific set of experiments was conducted to assess the possibility of regenerating and reusing TPEG for sequential treatments. In this regard, a chemical regeneration procedure was adopted. In particular, at the end of each adsorption test, the treated MB solution was completely drained from the pilot plant and the exhausted TPEG was left inside the column. Subsequently, a volume of 500 mL of a HCl (1 M) washing solution was recirculated through the column with a flowrate of 250 mL/min for 180 min. After this period, the washing solution was removed from the equipment and then distilled water was fed with the same flowrate for 60 min. The regenerated TPEG was reused in 5 adsorption cycles conducted at pH 11 and room temperature (20 ± 2 °C), by treating standard solutions with an initial MB concentration of 10 mg_{MB}/L. Each adsorption test was conducted as described in the previous paragraph.

The performance of regenerated TPEG was assessed by comparing the adsorption capacity detected in the initial test, conducted with the fresh material, with those monitored in the subsequent reusing tests. In this regard, the relative adsorption capacity q_R was considered:

$$q_R = \frac{MB\ adsorbed\ at\ a\ specific\ cycle\ (mg)}{MB\ adsorbed\ at\ the\ first\ use\ (mg)} \cdot 100 \quad (2)$$

2.5. Analytical methods and presentation of results

The concentration of methylene blue was measured at the wavelength of 664 nm, on a UV–visible spectrophotometer (Gan et al., 2018; Wang et al., 2020). Temperature and pH were monitored using bench analyzers.

Scanning electron microscopy (SEM) was used to analyze the morphology and structure of the TPEG. BET-N_2 (Brunauer–Emmett–-Teller) adsorption method was used to measure the specific surface area.

The pH of zero charge (pHzc) for TPEG was evaluated by two different methods. In the first one, different amounts of TPEG were put into pure water at solid to water ratios between 0.4% and 1.6%. The mixtures were stirred and the pH was checked after 24 h. The pHzc was identified with the stationary pH value (Cristiano et al., 2011). In the second procedure, a given amount TPEG (0.5 g) was added to 150 mL of solutions with different initial pH (between 2 and 13) and evaluating the final pH after 24 h of contact. The ΔpH observed for the different initial pH values was reported in a graph and the pHzc was identified as the point with ΔpH = 0 (Cristiano et al., 2011).

Each analysis was carried out in triplicate and the mean values with the standard deviation were reported in the graphs showing the MB removal.

2.6. Adsorption kinetic models

With the aim to pore over the mechanisms of MB adsorption on TPEG surface, a kinetic study was carried out. In this regard, the most common kinetic models reported in the literature were considered (Santoso et al., 2020). In particular, the experimental data were interpolated with a pseudo-first order model and a pseudo-second order model. In the general form, by referring to the concentration of contaminant in the solution, the pseudo-first order and pseudo-second order kinetics have

the following expressions, respectively (Siciliano et al., 2019):

$$\frac{dC}{dt} = -\overline{K}_1 \cdot (C - C_e) \tag{3}$$

$$\frac{dC}{dt} = -\overline{K}_2 \cdot (C - C_e)^2 \tag{4}$$

In these expressions C_e is the residual methylene blue at the equilibrium state, and $\overline{K}_1$ (min^{-1}) and $\overline{K}_2$ ($(mg_{MB}/L)^{-1}min^{-1}$) are the first-order and second-order observed kinetic constants.

The resolution of equations (3) and (4) provides the mathematical laws of C as a function of time:

$$C = C_i \cdot e^{-\overline{K}_1 \cdot t} + C_e \cdot \left(1 - e^{-\overline{K}_1 \cdot t}\right) \tag{5}$$

$$C = \frac{(C_i - C_e)}{1 + \overline{K}_2 \cdot (C_i - C_e) \cdot t} + C_e \tag{6}$$

in which C_i is the initial methylene blue concentration.

By referring to the specific adsorbed MB amount (q), the kinetic equations (3) and (4) become (Wang et al., 2020):

$$\frac{dq}{dt} = K_1 \cdot (q_e - q) \tag{7}$$

$$\frac{dq}{dt} = K_2 \cdot (q_e - q)^2 \tag{8}$$

where q_e is the adsorption capacity at the stationary state, K_1 (min^{-1}) and K_2 ($g_{TPEG}/(mg_{MB} \cdot min)$) are the kinetic constants referred to the MB adsorbed on the TPEG surface ($K_1 = \overline{K}_1$, $K_2 = \overline{K}_2 \frac{M_{TPEG}}{V}$). The resolution of equations (7) and (8) leads to the following expressions, respectively (Santoso et al., 2020; Wang et al., 2020):

$$q = q_e \cdot \left(1 - e^{-K_1 t}\right) \tag{9}$$

$$q = \frac{K_2 \cdot t \cdot q_e^2}{1 + K_2 \cdot t \cdot q_e} \tag{10}$$

2.7. Adsorption isotherms

Adsorption isotherms describe the distribution of the molecules of adsorbate between the solid and the liquid phase for a given temperature at the equilibrium state. Isotherms can give macroscopic information about the nature of the adsorption between the adsorbate and the adsorbent surface. As the two most exploited models for the fitting of isotherms are the Langmuir and Freundlich models, both were used to analyze the experimental data.

The Langmuir model is represented by equation (11):

$$q_e = q_{max} \frac{K_L \cdot C_e}{1 + K_L \cdot C_e} \tag{11}$$

where q_{max} (mg_{MB}/g_{TPEG}) is the maximum adsorption capacity, and K_L (L/mg_{MB}) is the Langmuir adsorption constant. This model assumes that the adsorption on a homogenous surface occurs through the formation of monolayer of adsorbates without further interactions between the adsorbates.

The Freundlich model is expressed as follows:

$$q_e = K_F \cdot C_e^{1/n} \tag{12}$$

in which K_F ($mg_{MB}^{1-1/n} \cdot L^{1/n}/g_{TPEG}$) is the Freundlich constant and 1/n is the adsorption strength, which indicates that the isotherm is irreversible (1/n = 0), favourable (0 < 1/n < 1) or unfavourable (1/n > 1) (Wang et al., 2020). The Freundlich expression assumes that the adsorption occurs on a heterogeneous surface and may involve a multilayer process.

The Redlich - Peterson model which incorporated the features of the Langmuir and Freundlich isotherms was also considered in this study:

$$q_e = \frac{K_{RP} \cdot C_e}{1 + a_{RP} \cdot C_e^{\beta}} \tag{13}$$

where K_{RP} (L/mg_{MB}) and a_{RP} $(L/mg_{MB})^{\beta}$ are the Redlich-Peterson constants, and β is an exponent which generally ranges between 0 and 1.

2.8. Thermodynamic analysis

The Gibbs energy change (ΔG°) reveals the level of spontaneity of an adsorption process. A more negative value indicates a more spontaneous and energetically favourable adsorption. ΔG° is expressed with the following law:

$$\Delta G^{\circ} = -R \cdot T \cdot lnK_a \tag{14}$$

where R is the universal gas constant (8.314 J/mol·K), T is the absolute temperature in kelvins, and K_a is the unitless thermodynamic equilibrium constant. As reported in section 3.6, the results obtained from the adsorption isotherms were used to estimate the values K_a and, consequently, of ΔG°.

3. Results and discussion

3.1. Characteristic of TPEG

TPEG is produced through an innovative industrial process from natural graphite by means of chemical intercalation followed by thermal plasma expansion at elevated temperature. This process separates graphite in many layers, with a volume expansion of up to 300 units. The thermo-plasma expansion conducted into an inert chamber ensures no oxidation of the graphite (Cuccarese et al., 2021). TPEG has dimensions between 60 and 300 μm and the total surface area resulted of about 46.5 m^2/g. This value is significantly higher than those reported for traditional thermo expanded graphite and GO-based materials (Fadillah et al., 2019; Wang et al., 2020; Chen et al., 2021).

The SEM images of TPEG show the presence of many sheets of graphene packed together forming a fibrous macrostructure (Fig. 2a). It can be noticed a crumpled structure which is common in graphene-type materials (Fig. 2b). Stacked sheets of various dimensions with a multilayered structure are present. The spacing between the sheets resulted approximately 20–60 nm (Fig. 2c).

A detailed characterization of the TPEG is reported in a previous work (Cuccarese et al., 2021).

The pH of zero charge was identified near 4 with both procedures applied . Indeed, by plotting the final pH recorded by increasing the TPEG to water ratio, a decreasing trend with an asymptotic value around 4 was detected (Figure S1a, supplementary material), which corresponds to the pHzc. The procedure at different initial pH values, in addition to the same pHzc, made it possible to obtain some other interesting information. The ΔpH was slightly positive when the pH was below 4, sharply decreasing to negative values above the pHzc and showing a point of minimum close to 11 (Figure S1b, supplementary material). Therefore, for pH > 4 the surface of the adsorbent assumes a negative charge which intensifies reaching the maximum negative value at a pH around 11. Above this point, the negative charge density becomes much weaker.

3.2. Adsorption tests conducted by varying the pH of the solution

The first experiments were conducted to assess the effect of pH on the adsorption process and to identify the optimal values to maximize the MB removal. In this regard, pH values from 5 to 13 were tested at T = 20 °C by treating solutions with MB initial concentrations of about 10 mg_{MB}/L. The curves of the MB residual concentration showed typical adsorption trends with an initial rapid decline, within the first 5 min of

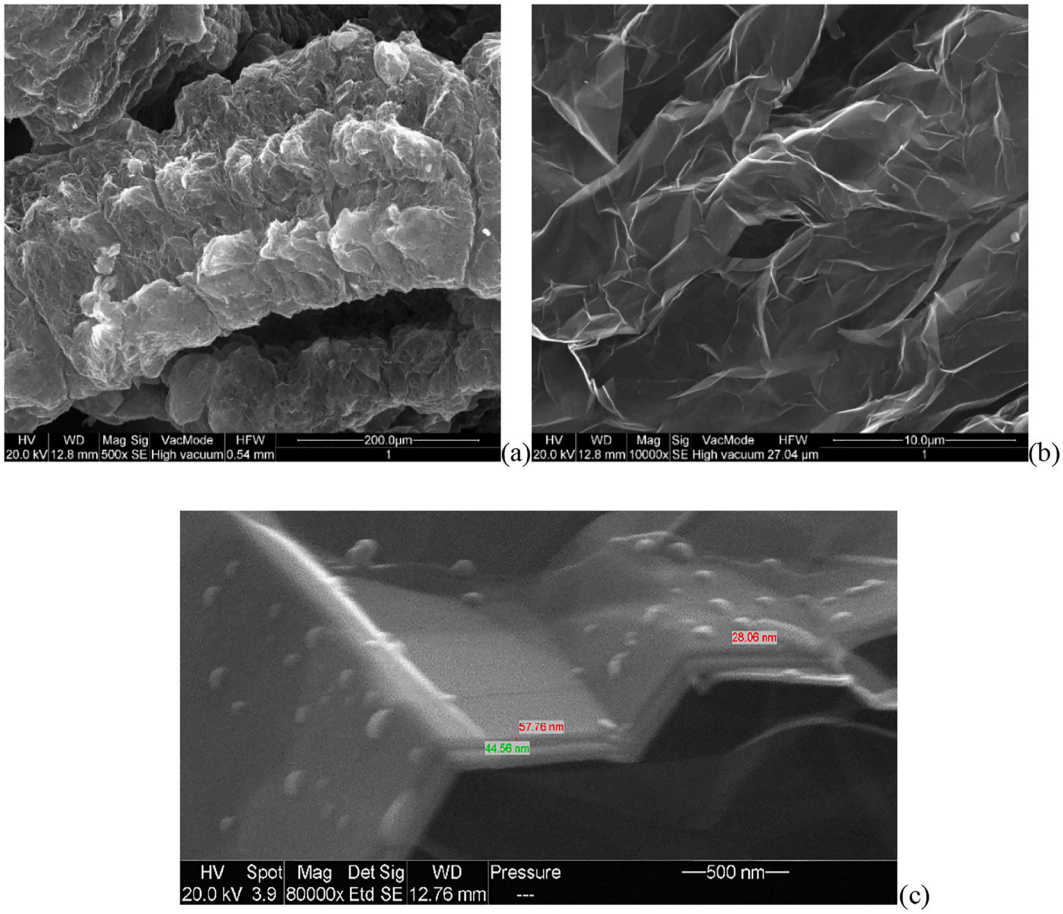

Fig. 2. SEM images of TPEG at different magnifications, 500× (a), 10000× (b), 80000× (c).

treatment, and a subsequent slower reduction, representative of a semi-stationary phase (Fig. 3a). The experimental results clearly show that the MB abatements was positively influenced by raising the pH of the solution (Fig. 3a). In particular, with pH values up to 9, concentrations higher than 6.5 mg_{MB}/L were monitored after 5 min, reaching MB removal comprised between 30% and 44% at the end of the treatment. The process efficiency notably grew by increasing the pH to 11, reaching concentration of about 4.5 mg_{MB}/L within the initial minutes and a final efficiency of about 74%, after 180 min (Fig. 3a). The adsorption of MB on TPEG was not further improved by raising the pH to 13 (Fig. 3a). At this value, anyhow, the adsorption process is affected by the modification of pollutant structure, as described below.

The notable improvement in the process performance in response to the pH growth to 11 is even more evident from the analysis of the trends

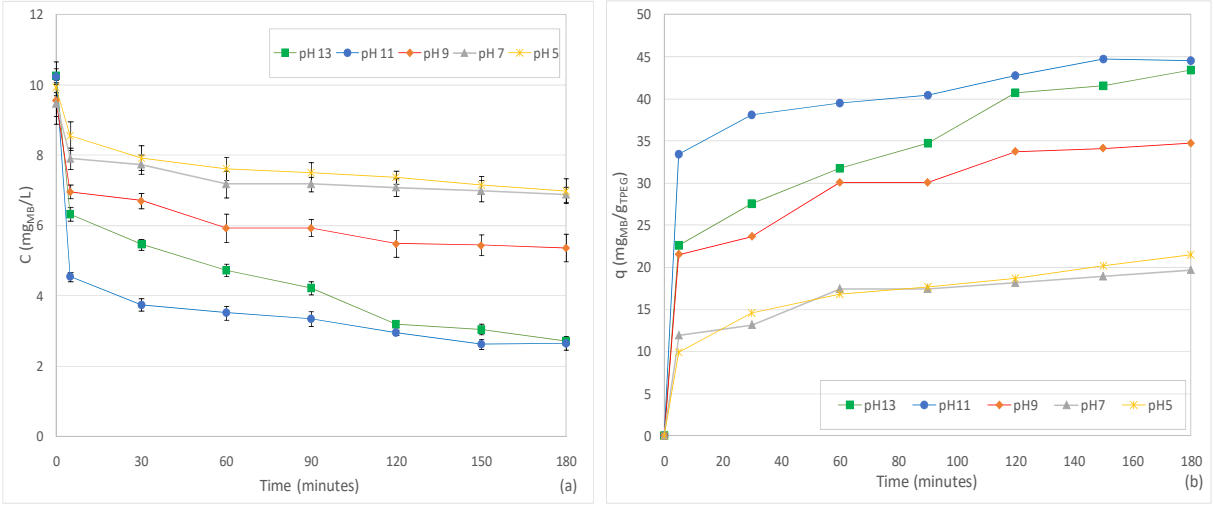

Fig. 3. Concentration of methylene blue (a) and specific adsorbed amount (b), during the tests carried out with T = 20 °C and by varying the pH (pH 5, M = 0.0684 g_{TPEG}; pH 7, M = 0.0660 g_{TPEG}; pH 9, M = 0.0605 g_{TPEG}; pH 11, M = 0.0850 g_{TPEG}; pH 13, M = 0.0876 g_{TPEG}). (For interpretation of the references to color in this figure legend, the reader is referred to the Web version of this article.)

of adsorbed amount (q). Indeed, the q value calculated at the end of the treatment, which represents the adsorption capacity (q_e), doubled as the pH increased from 5 to 11 (Fig. 3b).

The discussed results find a motivation by considering that, as previously discussed, the TPEG assumes a small positive charge for pH below 4, while above this value the adsorbent becomes negatively charged. The pH growth leads to an increase in the electronegativity of the adsorbent material surface, therefore, the electrostatic attraction of the MB, which is positively charged, is enhanced (Yang et al., 2011; Nayl et al., 2019) and the adsorption process becomes more effective. These findings clearly suggest that the electrostatic interaction is the predominant mechanism in the adsorption of MB on the surface of the TPEG. The maximum negative charge is reached around 11 which justifies the best adsorption performance found at this pH value. To further support these statements, as the MB could be hydrolysed in strong alkaline media, the spectra of standard MB solutions at pH 11 and 13 were detected over 3 h. At pH 13 it was observed a significant variation after 30 min (Figure S2, supplementary material). The detected spectra indicate the probable formation of Methylene Violet because of the hydrolysis of MB with alkali in aqueous solutions, in agreement with the statements of previous works (Adamčíková et al., 2000; Mills et al., 2011). However, the results show that the MB does not undergo substantial modifications at pH 11 (Figure S3, supplementary material) and, therefore, it keeps its molecular structure and positive charge. These observations confirm that at pH 11 the maximum absorption is imputable to the electrostatic attraction, while at higher pH the pollutant modification does not permit reliable considerations. High performances of the methylene blue adsorption process by graphene-based materials, at alkaline pH values, were also described by other works. Indeed, Zhang et al. (2011) reported similar results treating MB solutions characterised by graphene oxide in the pH range 2.7–11. In particular, the adsorption capacity linearly raised with increasing the solution pH up to 11 (Zhang et al., 2011). Furthermore, Yang et al. (2011) noticed an increase in the adsorption capacity by increasing the pH of the solution from 2 to 12 by exploiting graphene oxide. This effect was particularly appreciable at high initial MB concentrations; while, at lower concentrations, the adsorption capacity increased until the pH reached a threshold value and, then, remained almost constant (Yang et al., 2011).

However, other studies reported a negligible effect of the pH on the process. In particular, Liu et al. (2012) tested the influence of pH in the range 3–10 and noticed a minor variation in the removal rate, which increased only from 85.95% at pH 3, to 99.68% at pH 10. Li et al. (2013), while analysing three different carbonaceous materials (activated carbon, graphene oxide and multi-walled carbon nanotubes), found that the adsorption was not drastically influenced by pH. The different statements reported in the literature suggest that pH affects the removal of MB in different ways depending on the characteristics of the adsorbent exploited and the operating conditions applied. As mentioned above, in this study we found the pH 11 as the optimal value and, therefore, it was employed for all subsequent adsorption tests.

3.3. Adsorption tests conducted by varying the initial methylene blue concentration

Once identified the optimum pH, the subsequent experiments were carried out to spot the influence of initial dye concentration. In particular, five tests were executed by considering the concentrations of 2, 10, 20, 30 and 40 mg_{MB}/L.

As shown in Fig. 4a, decreasing efficiencies were detected while increasing the amount of methylene blue. Indeed, only in the case of the initial concentration equal to 2 mg_{MB}/L the dye was completely adsorbed within 90 min. On the contrary, by treating higher concentrations, the solutions still showed residual dye at the end of the process (Fig. 4a), with efficiencies that declined around to 55% and 40% in the tests with 30 mg_{MB}/L and 40 mg_{MB}/L, respectively. The deterioration in removal percentage is attributable to the progressive reduction of the available adsorption active sites at room temperature as the concentration increases. Indeed, the material's adsorption sites, as easily conceivable, at a given temperature gradually reach saturation due to the rise in the mass of the treated dye. On the other hand, when treating low MB amounts, the adsorption sites are not filled by the dye molecules and the removal efficiency improves (Zhang et al., 2011; Nayl et al., 2019).

The discussed results find a confirmation in the work of Nayl et al. (2019). The authors, by exploiting a sponge/oxide graphene composite, observed a decrease of the removal percentage from 99.3% to 41.3%, by increasing the concentration of methylene blue from 10 to 50 mg_{MB}/L (Nayl et al., 2019). Also, Zhang et al. (2011) and Wang et al. (2020) reported a great influence of the initial MB concentration on the adsorption process, by exploiting graphene oxide (Zhang et al., 2011) and graphene oxide modified persimmon tannins (Wang et al., 2020). Clearly, the quantity of dye that can be adsorbed is related to the properties and to the amount of the adsorbent material applied during the treatment. Indeed, for a given mass of the pollutant, increasing the quantity of the reactive material enhances the removal performance (Siciliano, 2015).

Although the removal percentage declined with the initial concentration, the adsorption capacity grew in response to the increase of the

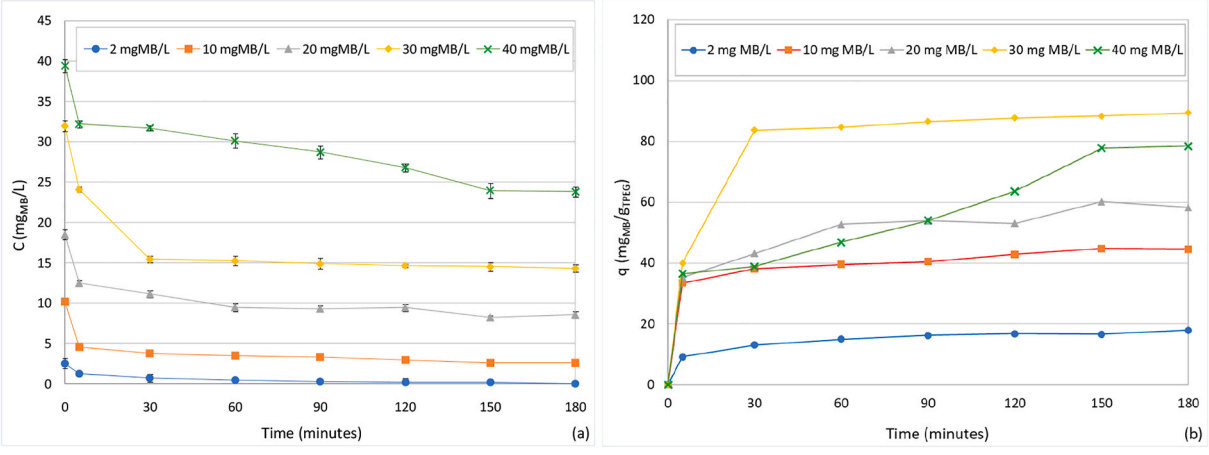

Fig. 4. Concentration of methylene blue (a) and specific adsorbed amount (b) during the tests carried out at pH = 11 and T = 20 °C, by varying the initial concentration of methylene blue (C_i = 2 mg_{MB}/L, M = 0.0697g_{TPEG}; C_i = 10 mg_{MB}/L, M = 0.0850g_{TPEG}; C_i = 20 mg_{MB}/L, M = 0.0854g_{TPEG}; C_i = 30 mg_{MB}/L, M = 0.1039g_{TPEG}; C_i = 40 mg_{MB}/L, M = 0.0992g_{TPEG}). (For interpretation of the references to color in this figure legend, the reader is referred to the Web version of this article.)

MB level and the highest value q_e = 89 mg_{MB}/g_{TPEG} was monitored in the test with 30 mg_{MB}/L (Fig. 4b). A slightly lower adsorption capacity was calculated for the test at 40 mg_{MB}/L. It is interesting to note how the adsorption capacity q_e, detected treating 30 mg_{MB}/L, was higher than the initial mass of dye in the test at 10 mg_{MB}/L and just slightly lower to that at 20 mg_{MB}/L. Therefore, it would be expected an almost complete adsorption of MB by treating concentrations lower than 30 mg_{MB}/L. Nevertheless, below this concentration, the total adsorbed amount of methylene blue was significantly lesser than the maximum adsorption capacity of the material. These findings suggest that the initial concentration provides a driving force able to overcome the mass transfer resistance between the solid and liquid phase and, therefore, allows larger quantities of dye to be adsorbed. On the other hand, by treating a low-concentrated solution, the limited mass of the dye produces a weak potential that does not permit to exploit the maximum adsorption capacity of the material. Such conditions were observed in previous research conducted by other authors (Wang et al., 2020).

3.4. Adsorption tests conducted at different temperatures

Further sets of tests were carried out by varying the process temperature. One set was conducted with the purpose of evaluating the performance of the treatment in a wide range of temperatures. For this reason, five tests by treating solutions with a concentration of about 10 mg_{MB}/L and by varying the temperature between 10 and 60 °C were executed. The trends reported in Fig. 5a showed a remarkable enhancement of MB removal yield by rising the temperature from 10 to 20 °C, with a jump of the MB abatement from 53% to 74%. (Fig. 5a). Few differences were observed in response to a further increase in temperature at 30 and 40 °C (Siciliano et al., 2021). Finally, the best performance was detected in the test conducted at 60 °C, in which almost the overall MB mass was adsorbed (Fig. 5a). However, at this temperature it was observed a variation in the coloration of the solution, which assumed a purple-blue shade. This effect was explained by the analysis of the absorption spectrum, which highlighted that the maximum wavelength was shifted from 664 nm, at room temperature, to 614 nm, at 60 °C. This behaviour was also reported by Nayl et al. (2019), who noticed a change in the colour intensity of the MB solution, when the temperature was raised to 70 °C, due to a reduction of the maximum wavelength from 664 nm, at 25 °C, to 618 nm, at 70 °C. Therefore, due to the modification of the methylene blue characteristics, the results at 60 °C were not considered attributable to an actual absorption process. The trends reported in Fig. 5b make it evident that the adsorption capacity notably increased as the temperature grew from 10 to 20 °C. However, beyond this temperature, by excluding the results at 60 °C, no further increases in the amount of MB adsorbed on the TPEG surface were observed (Fig. 5b). Indeed, taking into account the slight differences in the initial MB concentrations and in the mass of the adsorbent measured in each test, the actual quantities of MB adsorbed per unit of TPEG were very similar at temperatures between 20 and 40 °C. According to these results, when treating solutions with about 10 mg_{MB}/L, the temperature increase above the room condition is not able to induce a stronger driving force to enhance the adsorption capacity of TPEG.

To better understand the effects of temperature on the adsorption process, a further set of tests was conducted at 40 °C treating solutions with different concentrations. This permitted a comparison with the trends detected at 20 °C. The experimental results showed a marked effect of temperature on the adsorption process in the tests carried out with MB concentrations higher than 10 mg_{MB}/L (Fig. 6a). Indeed, compared to the results obtained at room temperature, the removal yields increased to about 84% by treating solutions with 20 mg_{MB}/L, and around 73% with initial concentrations of 30 and 40 mg_{MB}/L. The effect of temperature is evident by analysing the trends of the specific adsorbed amount (Fig. 6b). In fact, the values detected at the end of the treatment progressively increased with the initial MB concentration and were greater than those obtained at 20 °C in the tests with $C_i > 10$ mg_{MB}/L. It is interesting to note that, while at room temperature the highest adsorption capacity was detected by treating 30 mg_{MB}/L, at 40 °C the adsorption capacity continued to increase with the initial MB concentration. In particular, in the test with 40 mg_{MB}/L it was reached a final value, around 145 mg_{MB}/g_{TPEG}, 1.85 times higher than the adsorption capacity, of about 78.5 mg_{MB}/g_{TPEG}, detected with the same concentration at 20 °C. This difference finds a motivation considering that at room temperature the adsorption of MB could be hindered in high concentrated solutions by diffusive resistances towards the TPEG surface (Yao et al., 2010). In particular, the experimental results suggest that this effect occurs with concentrations above 30 mg_{MB}/L.

The increase in temperature causes a decrease in the solution viscosity and, therefore, a major diffusion of the adsorbate molecules across the boundary layer towards the external surface and in the internal pores of the adsorbent material (Al-Qodah, 2000; Hameed and Ahmad, 2009; Nayl et al., 2019; Yao et al., 2010). It is conceivable that this effect is more marked when treating high concentrated solutions, which justifies the higher adsorbed amount of MB detected by treating solutions with 40 mg_{MB}/L at 40 °C. This proves that the variation of temperature may change the adsorption capacity of the adsorbent towards a particular

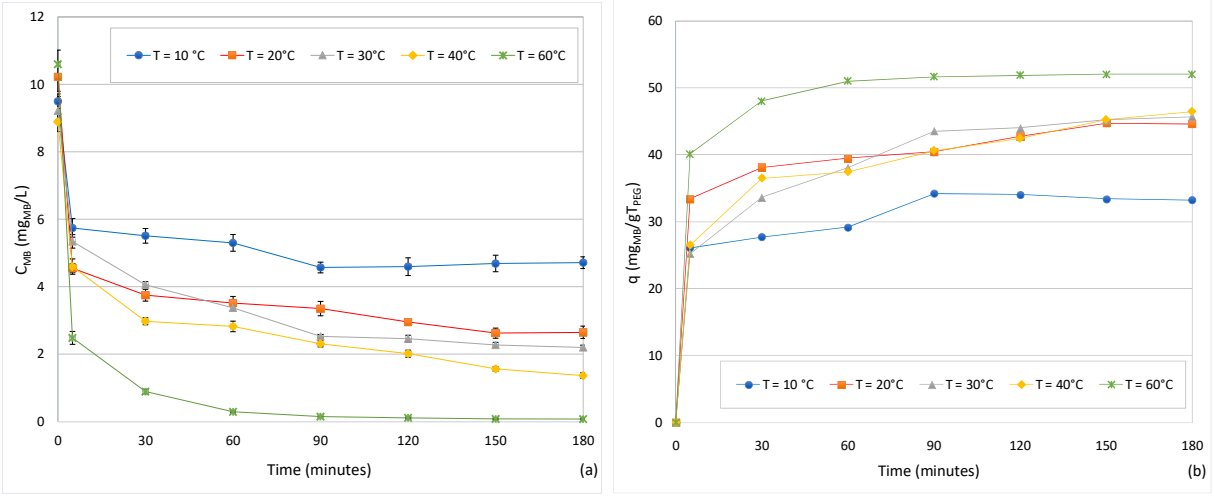

Fig. 5. Concentration of methylene blue (a) and specific adsorbed amount (b) during the tests carried out at pH 11 by treating solution with 10 mg MB/L and by varying the temperature (T = 10 °C, M = 0.072g_{TPEG}; T = 20 °C, M = 0.085g_{TPEG}; T = 30 °C, M = 0.077g_{TPEG}; T = 40 °C, M = 0.081g_{TPEG}; T = 60 °C, M = 0.101g_{TPEG}). (For interpretation of the references to color in this figure legend, the reader is referred to the Web version of this article.)

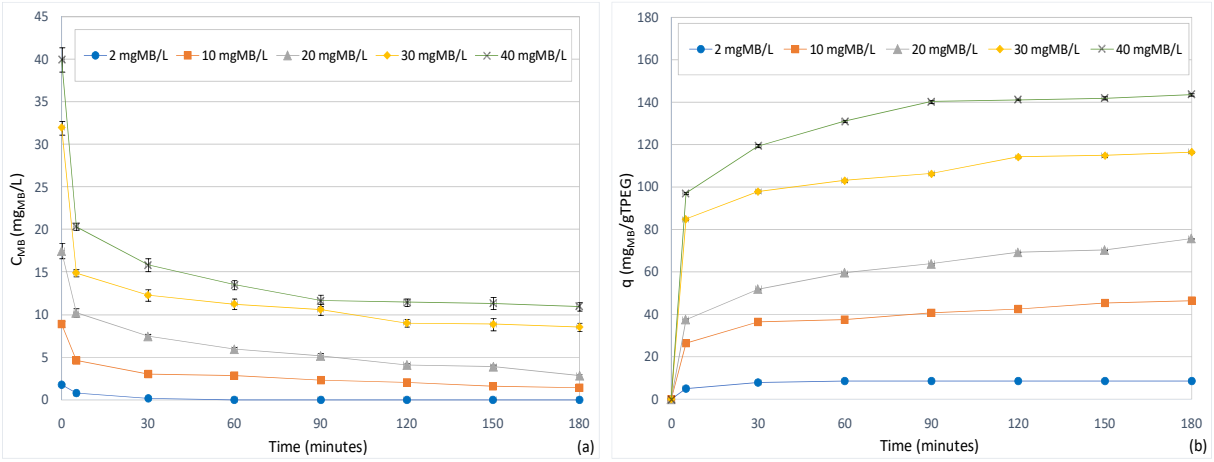

Fig. 6. Concentration of methylene blue (a) and specific adsorbed amount (b) during the tests carried out at pH = 11 and T = 40 °C, by varying the initial concentration of methylene blue (C_i = 2 mg_{MB}/L, M = 0.101g_{TPEG}; C_i = 10 mg_{MB}/L, M = 0.091 g_{TPEG}; C_i = 20 mg_{MB}/L, M = 0.0967 g_{TPEG}; C_i = 30 mg_{MB}/L, M = 0.100g_{TPEG}; C_i = 40 mg_{MB}/L, M = 0.101 g_{TPEG}). (For interpretation of the references to color in this figure legend, the reader is referred to the Web version of this article.)

adsorbate (Al-Qodah, 2000). In accordance with the results of the present study, Wang et al. (2020), using graphene oxide modified persimmon tannins, observed an increase of the equilibrium adsorption capacity with increasing temperature when initial concentrations beyond 10 mg_{MB}/L were treated. More in general, the positive effect of temperature on the adsorption process was previously reported by other authors, who exploited several materials for the removal of methylene blue dye. Hameed and Ahmad (2009), by using garlic peel for the adsorption of MB, noticed that the adsorption capacity increased from 82.64 mg/g to 142.86 mg/g when the temperature was increased from 303 to 323 K. Liu et al. (2012) reported an increase in the graphene adsorption capacity from 153.85 mg/g, at 293 K, to 204.08 mg/g, at 333 K.

3.5. Kinetic analysis

As previously stated (section 2.6), a kinetic analysis was conducted by referring to the pseudo-first order (Eqs. (5) and (9)) and pseudo-second order (Eqs. (6) and (10)) adsorption models. The interpolations of the experimental data with the two proposed kinetic laws are reported in the supplementary materials (Figures S4-S7). The kinetic parameters obtained from the interpolation of the experimental curves are reported in Tables 1–4. It must be underlined that the values of the adsorption capacity (q_e) were also obtained from the data simulations, without assuming them a priori from the observation of the monitored trends. By comparing the values of the R^2 for the two laws, it emerges that the best fitting was generally reached with the second order model. This is in agreement with many previous works (Santoso et al., 2020), although some papers reported other models as more appropriate kinetic laws (Tharaneedhar et al., 2017; Santoso et al., 2020). In effect, the adsorption kinetic could change in response to the type of adsorbent material and operating conditions applied.

According to the pseudo-second model found in this work (Eqs. (8) and (10)), the reaction rate largely depends on the adsorption capacity q_e. In fact, the adsorption evolves with the square of the difference between the adsorption capacity and the adsorbed amount at a given instant (Eqs. (8) and (10)). Thus, high values of q_e promote the adsorption rates. Obviously, both the adsorption capacity and the observed kinetic constant depend on the process operating conditions (pH, T, C_i). To make these relationships more evident, for each set of tests, the values of q_e and K_2 obtained from the interpolations of experimental data were plotted as a function of the operating parameters. The adsorption capacity and the kinetic constant rapidly grew in response to the pH increase attaining the highest values at a pH around 11 (Figs. 7a and 7b), which guarantees the greatest specific adsorption rate and adsorption capacity. The values at pH 13 are obviously affected by the modification of the pollutant in extremely high alkaline solutions.

The trends plotted in Fig. 8a show how the adsorption capacity increased with the initial concentration of methylene blue. On the contrary, with the rise in C_i the kinetic constant assumed decreasing trends (Fig. 8b). The opposite behaviors of q_e and K_2 indicate that the growth in the initial amount of methylene blue, as previously discussed, permits to exceed the mass transfer resistances and to adsorb higher quantities of the dye, even if overcoming these resistances slows the process. By comparing the results at 20 and 40 °C, it can be easily noticed that the trends of q_e overlap for initial MB level up to around 10 mg_{MB}/L (Fig. 8a). Above this concentration, a maximum value around to 86 mg_{MB}/g_{TPEG} was reached at T = 20 °C for C_i concentrations of about 30 mg_{MB}/L. With a temperature of 40 °C, instead, the adsorption capacity raised without attaining a threshold value. These results are in agreement with the statements of Wang et al. (2020) and indicate that the effect of temperature on the adsorption process becomes more pronounced as the amount of MB in the solution increases.

This is further confirmed by the adsorption capacity values identified

Table 1
Kinetic parameters obtained through the interpolation of the experimental curves of the tests at T = 20 °C, C_i = 10 mg_{MB}/L and by varying pH between 5 and 13.

T (°C)	pH	C_i (mg_{MB}/L)	M (g_{TPEG})	Pseudo-first order kinetic				Pseudo-second order kinetic				
				C_e (mg/L)	q_e (mg_{MB}/g_{TPEG})	$\overline{K}_1$ (min^{-1})	R^2	C_e (mg_{MB}/L)	q_e (mg_{MB}/g_{TPEG})	$\overline{K}_2$ (L/(mg_{MB}·min))	K_2 (g_{TPEG}/(mg_{MB}·min))	R^2
20	5	9.92	0.0684	7.37	18.62	0.1361	0.889	6.80	22.81	0.0224	0.00306	0.935
	7	9.47	0.0660	6.87	19.71	0.1717	0.723	6.91	19.43	0.0331	0.00437	0.940
	9	9.57	0.0605	5.81	31.08	0.2333	0.908	5.50	33.62	0.0480	0.00581	0.936
	11	10.22	0.0850	3.14	41.65	0.3229	0.975	3.02	42.35	0.0774	0.01316	0.984
	13	10.25	0.0876	3.88	36.36	0.1833	0.884	3.05	41.09	0.0139	0.00243	0.910

Table 2
Kinetic parameters obtained through the interpolation of the experimental curves of the tests at T = 20 °C, pH 11 and by varying C_i between 2 and 40 mg_{MB}/L.

T (°C)	pH	C_i (mg_{MB}/L)	M (g_{TPEG})	Pseudo-first order kinetic				Pseudo-second order kinetic				
				C_e (mg/L)	q_e (mg_{MB}/g_{TPEG})	$\overline{K}_1$ (min^{-1})	R^2	C_e (mg_{MB}/L)	q_e (mg_{MB}/g_{TPEG})	$\overline{K}_2$ (L/(mg_{MB}·min))	K_2 (g_{TPEG}/(mg_{MB}·min))	R^2
20	11	2.56	0.0697	0.34	15.94	0.1600	0.944	0.175	17.11	0.0785	0.0109	0.978
		10.22	0.0850	3.14	41.68	0.3232	0.975	3.020	42.41	0.0774	0.0132	0.983
		18.53	0.0854	9.37	53.59	0.2102	0.936	8.871	56.56	0.0282	0.0048	0.965
		31.98	0.1039	14.53	83.40	0.1172	0.989	14.04	86.38	0.0108	0.0022	0.990
		39.40	0.0992	24.35	75.85	0.0195	0.765	23.75	78.88	0.0041	0.0008	0.832

Table 3
Kinetic parameters obtained through the interpolation of the experimental curves from the tests at pH 11, with C_i = 10 mg_{MB}/L and by varying T between 10 and 60 °C.

T (°C)	pH	C_i (mg_{MB}/L)	M (g_{TPEG})	Pseudo-first order kinetic				Pseudo-second order kinetic				
				C_e (mg_{MB}/L)	q_e (mg_{MB}/g_{TPEG})	$\overline{K}_1$ (min^{-1})	R^2	C_e (mg_{MB}/L)	q_e (mg_{MB}/g_{TPEG})	$\overline{K}_2$ (L/(mg_{MB}·min))	K_2 (g_{TPEG}/(mg_{MB}·min))	R^2
10	11	9.50	0.072	4.89	31.96	0.3380	0.957	4.78	32.75	0.1413	0.0203	0.968
20		10.22	0.085	3.14	41.68	0.3229	0.975	2.97	42.67	0.0894	0.0152	0.983
30		9.22	0.077	2.81	41.72	0.2115	0.908	2.36	44.66	0.0304	0.0047	0.970
40		8.89	0.081	2.17	41.47	0.2010	0.950	1.81	43.70	0.0379	0.0061	0.970
60		10.59	0.101	0.58	49.51	0.2084	0.994	0.04	52.21	0.0607	0.0123	0.999

Table 4
Kinetic parameters obtained through the interpolation of the experimental curves of the tests at T = 40 °C, pH 11 and by varying C_i between 2 and 40 mg_{MB}/L.

T (°C)	pH	C_i (mg_{MB}/L)	M (g_{TPEG})	Pseudo-first order kinetic				Pseudo-second order kinetic				
				C_e (mg_{MB}/L)	q_e (mg_{MB}/g_{TPEG})	$\overline{K}_1$ (min^{-1})	R^2	C_e (mg_{MB}/L)	q_e (mg_{MB}/g_{TPEG})	$\overline{K}_2$ (L/(mg_{MB}·min))	K_2 (g_{TPEG}/(mg_{MB}·min))	R^2
40	11	1.73	0.1010	0.022	8.46	0.1746	0.994	$3{\cdot}10^{-14}$	8.57	0.1782	0.0360	0.993
		8.89	0.0911	2.17	36.88	0.2013	0.950	1.8	38.86	0.0379	0.0069	0.973
		17.49	0.0967	4.85	65.36	0.1616	0.918	3.83	70.67	0.0128	0.0025	0.961
		31.98	0.1007	10.08	108.76	0.3024	0.973	9.49	111.71	0.0251	0.0050	0.983
		39.96	0.1011	12.26	137.00	0.2451	0.969	11.18	142.35	0.0132	0.0027	0.985

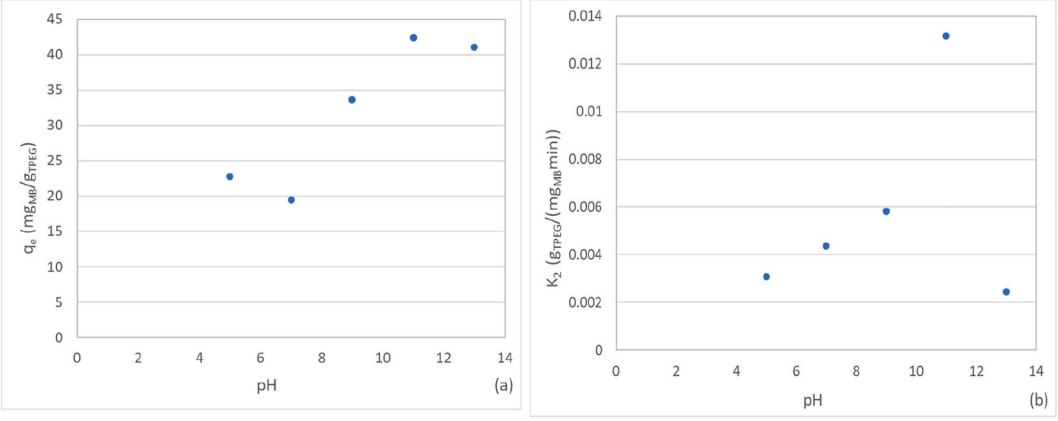

Fig. 7. Adsorption capacity vs. pH (a) and kinetic constant K_2 vs. pH (b). Data obtained through the interpolation of the experimental curves of the tests at T = 20 °C, C_i = 10 mg_{MB}/L and by varying pH between 5 and 13.

by the interpolations of the experiments carried out by treating solutions with 10 mg_{MB}/L and changing the temperature between 10 and 60 °C (Fig. 9a). In fact, a significant enhancement in the adsorption capacity was only obtained by increasing the temperature from 10 to 20 °C (Fig. 9a), and no improvements were observed at 30 and 40 °C. As mentioned in paragraph 3.4, the results at 60 °C are not reliable due to change in the properties of methylene blue. Furthermore, it must be noticed that the increase in temperature corresponds to a decline in the specific reaction rate (K_2) (Fig. 9b). This decline in the kinetic constant may be attributable to a higher incidence of desorption mechanisms when a temperature increase occurs. Nevertheless, the higher values of q_e detected at T ≥ 20 °C allow the process to evolve with an overall reaction rate similar to that at 10 °C.

3.6. Adsorption isotherms

The adsorption isotherms were identified for the temperatures of 20 and 40 °C by referring to the Langmuir, Freundlich and Redlich-Peterson models (Eqs. (11)–(13)) (Section 2.7). In this regard, the values of q_e and C_e obtained from the interpolation of the experimental adsorption

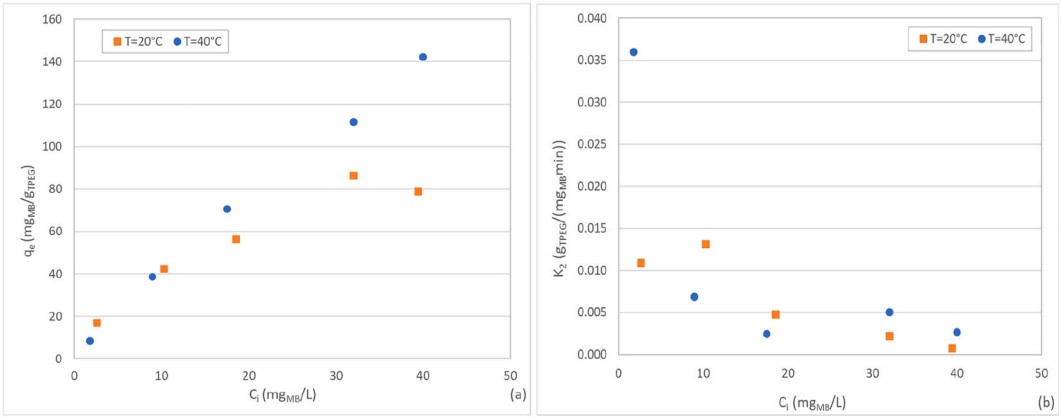

Fig. 8. Adsorption capacity vs. C_i (a) and kinetic constant K_2 vs. C_i (b). Data obtained through the interpolation of the experimental curves of the tests at pH = 11 for T = 20 °C and T = 40 °C.

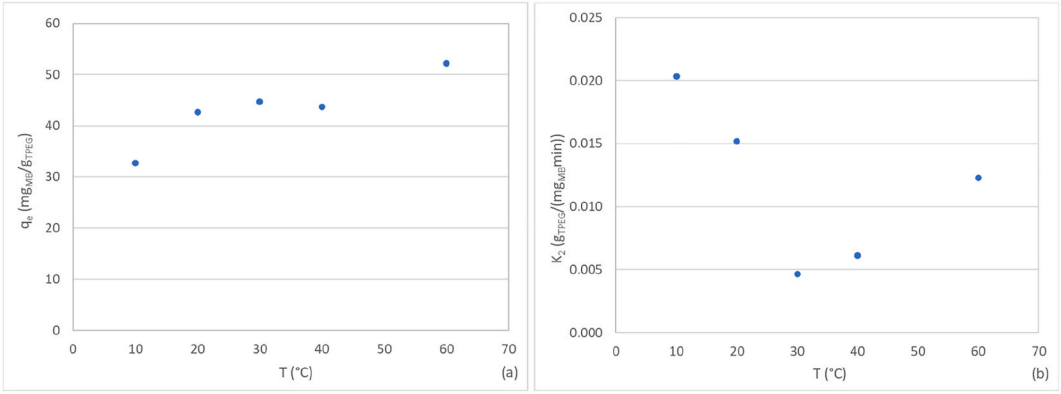

Fig. 9. Adsorption capacity vs. T (a) and kinetic constant K_2 vs. T (b). Data obtained through the interpolation of the experimental curves of the tests at pH = 11, C_i = 10 mg_{MB}/L, and by varying T between 10 and 60 °C.

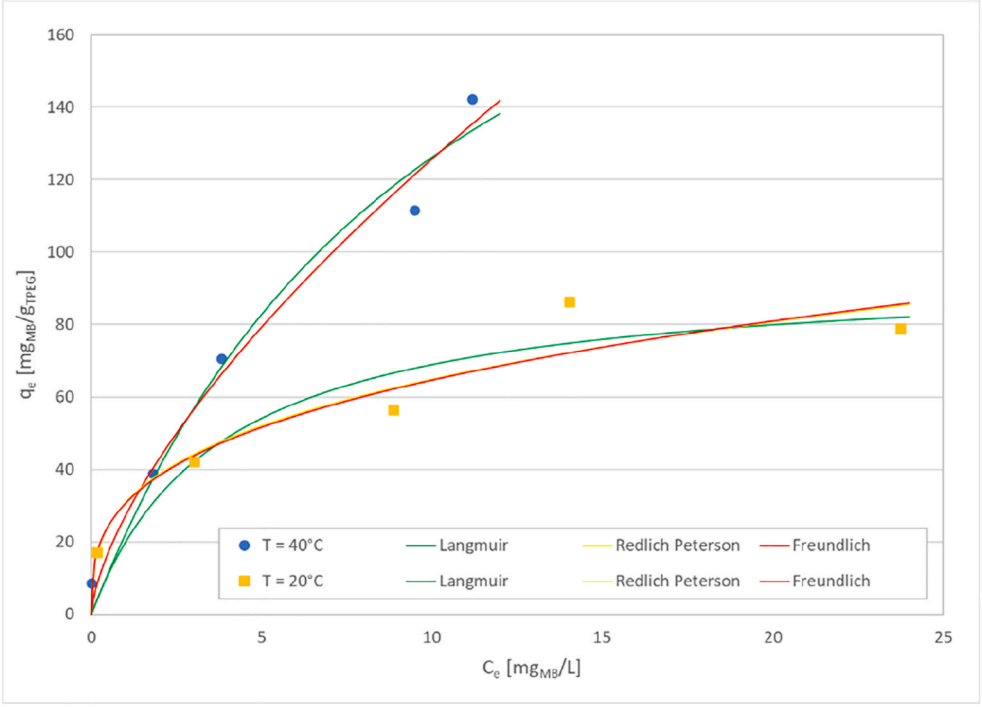

Fig. 10. Identification of isotherms at 20 °C and 40 °C.

curves were used (Tables 1–4). The fitting of the experimental data with equations (11)–(13) is shown in Fig. 10. The values of the parameters of the three models, obtained through the interpolations, are reported in Table 5.

In terms of the values of R^2, very similar fittings were obtained with the three isotherms analysed. In effect, just a slight difference was detected between the Freundlich and Langmuir isotherms. In particular, the Freundlich model fits slightly better at experimental points near the origin of the axes, while Langmuir law seems to be a bit more reliable for the higher values. Moreover, the analogous values of R^2 obtained with the Redlich e Peterson model, which is a combination of the other two isotherms, confirm that the adsorption process evolves according to both the features of Freundlich and Langmuir laws. The trends of the isotherms make clear how the temperature enhances the equilibrium adsorption capacity when high levels of MB are present in the liquid phase. In other works, an opposite behaviour was observed (Gan et al., 2018; Wang et al., 2020), which underlines how the adsorbent materials are differently affected by temperature in terms of adsorption capacity. In the present study, the maximum value of q_e estimated with the Langmuir law was about 95 mg_{MB}/g_{TPEG} and 265 mg_{MB}/g_{TPEG} at 20 and 40 °C. These values are higher than those detected for modified GO particles (Fadillah et al., 2019; Wang et al., 2020) and natural adsorbent materials (Hameed and Ahmad, 2009), which proves the effectiveness of TPEG in the removal of MB.

The equilibrium parameters derived from the Langmuir isotherm can be effectively exploited in thermodynamic analysis for the calculation of changes in free energy (ΔG°) (Eq. (14)) (Karaer and Kaya, 2016; Wang et al., 2020).

By assuming $Ka = K_L \cdot q_{max}$ (Karaer and Kaya, 2016; Wang et al., 2020) in equation (14), the values of ΔG° resulted equal to −7.85 kJ/mol and −7.75 kJ/mol at 20 and 40 °C, respectively, which prove that the adsorption process of methylene blue on TPEG is a spontaneous process. The ΔG° values, comprised between −20 and 0 kJ/mol, imply that the physisorption interactions are predominant (Santoso et al., 2020). The negligible difference between the values obtained at 20 and 40 °C, indicates that the temperature does not induce notable modifications from the thermodynamics perspective. In effect, the temperature increase, as above discussed, enhances the adsorption capacity but, on the other hand, the threshold value (q_{max}) can be attained at lower C_e concentrations at room temperature (Fig. 10). The similar values of ΔG° do not permit to evaluate the variation of enthalpy and entropy of the process.

3.7. Reuse of regenerated TPEG

The potential reuse of the adsorbent material in subsequent treatments is an important aspect for practical applications.

The values of q_R (Eq. (2)) reported in Fig. 11 clearly show that the chemical regeneration of the adsorbent material with HCl did not cause any reduction of the adsorption capacity for two cycles after the first use of fresh TPEG. Indeed, even higher amounts of adsorbed MB were monitored up to the 2nd reuse. A decrease of the adsorption capacity occurred from the 3rd reuse, with q_R values that resulted around 80% and remained stable until the last cycle.

These findings prove that the chemical regeneration is a suitable method that allows for effective reuse of TPEG in the removal of MB. In effect, the HCl used as a washing solution causes a complete desorption of dye without damaging the TPEG's surface. On the contrary, in a previous work it was observed a dramatic reduction of the adsorption capacity in the removal of diclofenac by applying a solvent washing with the TPEG stirred in a NaOH solution (Cuccarese et al., 2021). Much better results were detected with a thermal regeneration procedure, which, however, would result in a very expensive treatment (Cuccarese et al., 2021). The authors argued that the solubility of diclofenac in basic solutions is not enough to obtain an effective desorption with chemical washing. The decrease of relative adsorption capacity was also justified by the material loss during the separation of TPEG from the treated solution, after the adsorption process, and from the washing solution, at the end of regeneration step (Cuccarese et al., 2021). These drawbacks can be prevented with the column configuration used in the present study. In fact, during the adsorption treatment and the regeneration procedure, the adsorbed material is retained inside the column and, therefore, the difficulties and risks associated with the solid-liquid separation phases are completely avoided. Moreover, in the column system the chemical regeneration results in an easier and simpler procedure. Therefore, the developed system facilitates the application of graphene-type materials in the adsorption treatment.

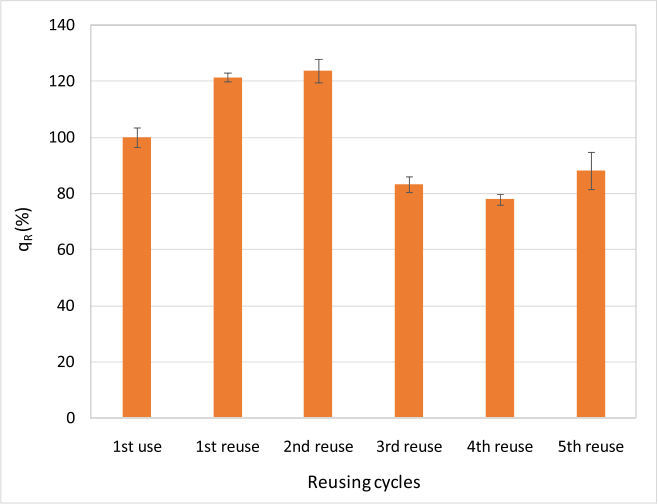

Fig. 11. Relative adsorption capacity during the reusing cycles of TPEG.

4. Conclusions

In the present study, the adsorption of methylene blue on thermo plasma expanded graphite, fixed in a new multilayer column system, was analysed. The experiments were conducted with the aim to identify the effects of pH, initial MB concentration and temperature on the adsorption process. The process was analysed in batch mode and the evolution over time was assessed.

The main adsorption mechanism was identified in the electrostatic interaction. Indeed, increasing performances were monitored in response to pH rise up to a value of about 11, at which the TPEG shows the higher negative charge. At room temperature, the adsorption capacity reached the highest value by treating solutions characterized by a concentration close to 30 mg_{MB}/L. The temperature increase above 20 °C produced an appreciable enhancement in the amount of MB that

Table 5
Isotherms parameters for the adsorption of MB, with Langmuir, Freundlich and Redlich-Peterson models.

T (°C)	Langmuir			Freundlich			Redlich-Peterson			
	q_{max} (mg_{MB}/g_{TPEG})	K_L (L/mg_{MB})	R^2	K_F ($mg_{MB}^{1-1/n} \cdot L^{1/n}/g_{TPEG}$)	n	R^2	K_{RP} (L/mg_{MB})	a_{RP} (L/mg_{MB})$^{\beta}$	β	R^2
20	94.92	0.2649	0.907	30.66	3.082	0.911	829.6	25.88	0.6896	0.911
40	265.2	0.0909	0.976	27.21	1.505	0.979	4228	154.5	0.3368	0.979

can be adsorbed when treating concentrations greater than 10 mg_{MB}/L.

Through a kinetic analysis it was found that the adsorption process can be represented with a pseudo second-order model and the kinetic constants were correlated with the operating parameters. The adsorption isotherms were defined for the temperatures of 20 and 40 °C by referring to different models. The interpolations suggested that the adsorption process evolves according to both the features of Freundlich and Langmuir laws. The maximum adsorption capacities was calculated around to 95 mg_{MB}/g_{TPEG} and 265 mg_{MB}/g_{TPEG} at 20 and 40 °C, respectively, which were higher than those of other types of graphene materials. From the values of ΔG° it was realized that the adsorption of methylene blue on TPEG is a spontaneous process. Finally, it was demonstrated that TPEG can be effectively reused at least 5 times in sequential cycles after a simple chemical regeneration procedure. This is a meaningful aspect as it allows treating high volumes of wastewater with the same TPEG amount, notably reducing the consumption of the adsorbent. Therefore, the detected results proved that the thermo plasma expanded graphite is an effective adsorbent material for the removal of methylene blue. The use of TPEG is favoured by the multi-layer column system developed and applied in this study, as it avoids the loss of material from treating units and facilitates the regeneration procedure. This can lead to notable environmental benefits by allowing the effective removal of a worrisome pollutant without the potential drawbacks connected to the use of graphene materials in conventional reactors.

Despite these considerations, further research is necessary to optimize the operation conditions for applications in real plants. In particular, in order to reduce the consumption of alkali reagents, the CO_2 stripping through air insufflations for a partial correction of pH could be a suitable approach. Moreover, the use of a flux of hot air would also allow the heating of the solution up to reach the temperatures required in the treatment of high MB concentrations (>10mg_{MB}/L). In addition to these aspects, studies can be conducted to further develop the TPEG (eg. through magnetization or by fixing reactive nanoparticles on its surface) and, subsequently, to assess the ability in the adsorption of MB. Finally, it would be very interesting to test the TPEG and TPEG-based materials in the removal of other types of contaminants.

Credit author statement

Alessio Siciliano: Conceptualization, Methodology, Data curation, Writing-Review and Editing; Giulia Maria Curcio: Methodology, Investigation, Data curation, Writing-Review and Editing; Carlo Limonti: Investigation, Data curation. Salvatore Masi: Conceptualization, Writing-Review and Editing. Michele Greco: Conceptualization, Writing-Review and Editing.

Funding

This research did not receive any specific grant from funding agencies in the public, commercial, or not-for-profit sectors.

Declaration of competing interest

The authors declare that they have no known competing financial interests or personal relationships that could have appeared to influence the work reported in this paper.

Appendix A. Supplementary data

Supplementary data to this article can be found online at https://doi.org/10.1016/j.jenvman.2021.113365.

References

Adamčíková, L.'U., Pavlíková, K., Ševčík, P., 2000. The decay of methylene blue in alkaline solution. Kluwer Academic Publisher & Akadémiai Kiadó 69, 91–94.
Aksu, Z., 2005. Application of biosorption for the removal of organic pollutants: a review. Process Biochem. 40, 997–1026. https://doi.org/10.1016/j.procbio.2004.04.008.
Almeida, C.A.P., Debacher, N.A., Downs, A.J., Cottet, L., Mello, C.A.D., 2009. Removal of methylene blue from colored effluents by adsorption on montmorillonite clay. J. Colloid Interface Sci. 332, 46–53. https://doi.org/10.1016/j.jcis.2008.12.012.
Al-Qodah, Z., 2000. Adsorption of dyes using shale oil ash. Water Res. 34 (17), 4295–4303. https://doi.org/10.1016/S0043-1354(00)00196-2.
Anirudhan, T.S., Ramachandran, M., 2015. Adsorptive removal of basic dyes from aqueous solutions by surfactant modified bentonite clay(organoclay): kinetic and competitive adsorption isotherm. Process Saf. Environ. Protect. 95, 215–225. https://doi.org/10.1016/j.psep.2015.03.003.
Calimli, M.H., Nas, M.S., Buran, H., Mustafov, S.D., Demirbas, Ö., Sen, F., 2020. Preparation, characterization and adsorption kinetics of methylene blue dye in reduced-graphene oxide supported nanoadsorbents. J. Mol. Liq. 309, 113171. https://doi.org/10.1016/j.molliq.2020.113171.
Caniani, D., Calace, S., Mazzone, G., Caivano, M., Mancini, I.M., Greco, M., Masi, S., 2018. Removal of hydrocarbons from contaminated soils by using a thermally expanded graphite sorbent. Bull. Environ. Contam. Toxicol. 101, 698–704. https://doi.org/10.1007/s00128-018-2395-4.
Chandra, V., Park, J., Chun, Y., Woo Lee, J., Hwang, I.C., Kim, K.S., 2010. Water-dispersible magnetite-reduced graphene oxide composites for arsenic removal. ACS Nano 4 (7), 3979–3986. https://doi.org/10.1021/nn1008897.
Chen, X., Xiao, F., Lei, Y., Lu, H., Zhang, J., Yan, M., Xu, J., 2021. A novel approach for synthesis of expanded graphite and its enhanced lithium storage properties. Journal of Energy Chemistry 59, 292–298. https://doi.org/10.1016/j.jechem.2020.10.006.
Cristiano, E., Hu, Y.-J., Siegfried, M., Kaplan, D.I., Nitsche, H., 2011. A comparison of point of zero charge measurement methodology. Clay Clay Miner. 59 (2), 107–115. https://doi.org/10.1346/CCMN.2011.0590201.
Cuccarese, M., Brutti, S., De Bonis, A., Teghil, R., Mancini, I.M., Masi, S., Caniani, D., 2021. Removal of diclofenac from aqueous solutions by adsorption on thermo-plasma expanded graphite. Sci. Rep. 11, 3427. https://doi.org/10.1038/s41598-021-83117-z.
Deng, H., Yang, L., Tao, G., Dai, J., 2009. Preparation and characterization of activated carbon from cotton stalk by microwave assisted chemical activation - application in methylene blue adsorption from aqueous solution. J. Hazard Mater. 166, 1514–1521. https://doi.org/10.1016/j.jhazmat.2008.12.080.
Deng, H., Lu, J., Li, G., Zhang, G., Wang, X., 2011. Adsorption of methylene blue on adsorbent materials produced from cotton stalk. Chem. Eng. J. 172, 326–334. https://doi.org/10.1016/j.cej.2011.06.013.
Dural, M.U., Cavas, L., Papageorgiou, S.K., Katsaros, F.K., 2011. Methylene blue adsorption on activated carbon prepared from Posidonia oceanica (L.) dead leaves: kinetics and equilibrium studies. Chem. Eng. J. 168, 77–85. https://doi.org/10.1016/j.cej.2010.12.038.
Fadillah, G., Saleh, T.A., Wahyuningsih, S., Putri, E.N.K., Febrianastuti, S., 2019. Electrochemical removal of methylene blue using alginate-modified graphene adsorbents. Chem. Eng. J. 378, 122140 ttps://doi.org/10.1016/j.cej.2019.122140.
Forgacs, E., Cserháti, T., Oros, G., 2004. Removal of synthetic dyes from wastewaters: a review. Environ. Int. 30, 953–971. https://doi.org/10.1016/j.envint.2004.02.001.
Fu, Y., Viraraghavan, T., 2001. Fungal decolorization of wastewaters: a review. Bioresour. Technol. 79, 251–262. https://doi.org/10.1016/S0960-8524(01)00028-1.
Gan, D., Liu, M., Huang, H., Chen, J., Dou, J., Wen, Y., Huang, Q., Yang, Z., Zhang, X., Wei, Y., 2018. Facile preparation of functionalized carbon nanotubes with tannins through mussel-inspired chemistry and their application in removal of methylene blue. J. Mol. Liq. 271, 246–253. https://doi.org/10.1016/j.molliq.2018.08.079.
Hameed, B.H., Din, A.T.M., Ahmad, A.L., 2007. Adsorption of methylene blue onto bamboo-based activated carbon: kinetics and equilibrium studies. J. Hazard Mater. 141, 819–825. https://doi.org/10.1016/j.jhazmat.2006.07.049.
Hameed, B.H., Ahmad, A.A., 2009. Batch adsorption of methylene blue from aqueous solution by garlic peel, an agricultural waste biomass. J. Hazard Mater. 164, 870–875. https://doi.org/10.1016/j.jhazmat.2008.08.084.
Karaer, H., Kaya, I., 2016. Synthesis, characterization of magnetic chitosan/active charcoal composite and using at the adsorption of methylene blue and reactive blue4. Microporous Mesoporous Mater. 232, 26–38. https://doi.org/10.1016/j.micromeso.2016.06.006.
Khare, N., Bajpai, J., Bajpai, A.K., 2018. Graphene coated iron oxide (GCIO) nanoparticles as efficient adsorbent for removal of chromium ions: preparation, characterization and batch adsorption studies. Environmental Nanotechnology, Monitoring & Management 10, 148–162. https://doi.org/10.1016/j.enmm.2018.06.002.
Li, X., Ai, L., Jiang, J., 2016. Nanoscale zerovalent iron decorated on graphene nanosheets for Cr(VI) removal from aqueous solution: surface corrosion retard induced the enhanced performance. Chem. Eng. J. 288, 789–797. https://doi.org/10.1016/j.cej.2015.12.022.
Li, Y., Du, Q., Liu, T., Peng, X., Wang, J., Sun, J., Wang, Y., Wu, S., Wang, Z., Xia, Y., Xia, L., 2013. Comparative study of methylene blue dye adsorption onto activated carbon, graphene oxide, and carbon nanotubes. Chem. Eng. Res. Des. 91 (2), 361–368. https://doi.org/10.1016/j.cherd.2012.07.007.
Liu, F., Yang, J.H., Zuo, J., Ma, D., Gan, L., Xie, B., Wang, P., Yang, B., 2014. Graphene-supported nanoscale zero-valent iron: removal of phosphorus from aqueous solution

and mechanistic study. J. Environ. Sci. 26, 1751–1762. https://doi.org/10.1016/j.jes.2014.06.016.
Liu, S., Ge, H., Wang, C., Zou, Y., Liu, J., 2018. Agricultural waste/graphene oxide 3D bio-adsorbent for highly efficient removal of methylene blue from water pollution. Sci. Total Environ. 628–629, 959–968. https://doi.org/10.1016/j.scitotenv.2018.02.134.
Liu, T., Li, Y., Du, Q., Sun, J., Jiao, Y., Yang, G., Wang, Z., Xia, Y., Zhang, W., Wang, K., Zhu, H., Wu, D., 2012. Adsorption of methylene blue from aqueous solution by graphene. Colloids Surf. B Biointerfaces 90, 197–203. https://doi.org/10.1016/j.colsurfb.2011.10.019.
Marrakchi, F., Ahmed, M.J., Khanday, W.A., Asif, M., Hameed, B.H., 2017. Mesoporous-activated carbon prepared from chitosan flakes via single-step sodium hydroxide activation for the adsorption of methylene blue. Int. J. Biol. Macromol. 98, 233–239. https://doi.org/10.1016/j.ijbiomac.2017.01.119.
Mills, A., Hazafy, D., Parkinson, J., Tuttle, T., Hutchings, M.G., 2011. Effect of alkali on methylene blue (C.I. Basic Blue 9) and other thiazine dyes. Dyes Pigments 88, 149–155. https://doi.org/10.1016/j.dyepig.2010.05.015.
Mossa Hosseini, S., Ataie-Ashtiani, B., Kholghi, M., 2011. Nitrate reduction by nano-Fe/Cu particles in packed column. Desalination 276, 214–221. https://doi.org/10.1016/j.desal.2011.03.051.
Nayl, A.A., Abd-Elhamid, A.I., El-Shanshory, A.A., Soliman, H.M.A., Kenawy, E.R., Aly, H.F., 2019. Development of sponge/graphene oxide composite as eco-friendly filter to remove methylene blue from aqueous media. Appl. Surf. Sci. 496, 143676. https://doi.org/10.1016/j.apsusc.2019.143676.
Pascale, R., Bianco, G., Calace, S., Masi, S., Mancini, I.M., Mazzone, G., Caniani, D., 2018. Method development and optimization for the determination ofbenzene, toluene, ethylbenzene and xylenes in water at trace levels by static headspace extraction coupled to gaschromatography–barrier ionization discharge detection. J. Chromatogr. 1548, 10–18. https://doi.org/10.1016/j.chroma.2018.03.018.
Peres, E.C., Slaviero, J.C., Cunha, A.M., Hosseini–Bandegharaei, A., Dotto, G.L., 2018. Microwave synthesis of silica nanoparticles and its application for methylene blue adsorption. J. Environ. Chem. Eng. 6, 649–659. https://doi.org/10.1016/j.jece.2017.12.062.
Rafatullah, M., Sulaiman, O., Hashim, R., Ahmad, A., 2010. Adsorption of methylene blue on low-cost adsorbents: a review. J. Hazard Mater. 177 (1–3), 70–80. https://doi.org/10.1016/j.jhazmat.2009.12.047.
Robinson, T., McMullan, G., Marchant, R., Nigam, P., 2001. Remediation of dyes in textile effluent: a critical review on current treatment technologies with a proposed alternative. Bioresour. Technol. 77, 247–255. https://doi.org/10.1016/S0960-8524(00)00080-8.
Ruan, W., Hu, J., Qi, J., Hou, Y., Cao, R., Wei, X., 2018. Removal of crystal violet by using reduced-graphene-oxide-supported bimetallic Fe/Ni nanoparticles (rGO/Fe/Ni): application of artificial intelligence modeling for the optimization process. Materials 11, 865. https://doi.org/10.3390/ma11050865.
Santoso, E., Ediati, R., Kusumawati, Y., Bahruji, H., Sulistiono, D.O., Prasetyoko, D., 2020. Review on recent advances of carbon based adsorbent for methylene blue removal from waste water. Materials Today Chemistry 16, 100233. https://doi.org/10.1016/j.mtchem.2019.100233.
Siciliano, A., 2015. Use of nanoscale zero-valent iron (NZVI) particles for chemical denitrification under different operating conditions. Metals 5 (3), 1507–1519. https://doi.org/10.3390/met5031507.
Siciliano, A., 2016. Removal of Cr(VI) from water using a new reactive material: magnesium oxide supported nanoscale zero-valent iron. Materials 9 (8), 666. https://doi.org/10.3390/ma9080666.
Siciliano, A., Curcio, G.M., Limonti, C., 2021. Hexavalent chromium reduction by zero-valent magnesium particles in column systems. J. Environ. Manag. 293, 112905 https://doi.org/10.1016/j.jenvman.2021.112905.
Siciliano, A., Limonti, C., 2018. Nanoscopic zero-valent iron supported on MgO for lead removal from waters. Water 10 (4), 404. https://doi.org/10.3390/w10040404.
Siciliano, A., Curcio, G.M., Limonti, C., 2019. Experimental analysis and modeling of nitrate removal through zero- valent magnesium particles. Water 11 (6), 1276. https://doi.org/10.3390/w11061276.
Siciliano, A., Curcio, G.M., Limonti, C., 2020. Chemical denitrification with Mg0 particles in column systems. Sustainability 12, 2984. https://doi.org/10.3390/su12072984.
Singh, K., Arora, S., 2011. Removal of synthetic textile dyes from wastewaters: a critical review on present treatment technologies. Crit. Rev. Environ. Sci. Technol. 41 (9), 807–878. https://doi.org/10.1080/10643380903218376.
Sun, Y., Ding, C., Cheng, W., Wang, X., 2014. Simultaneous adsorption and reduction of U(VI) on reduced graphene oxide-supported nanoscale zerovalent iron. J. Hazard Mater. 280, 399–408. https://doi.org/10.1016/j.jhazmat.2014.08.023.
Tharaneedhar, V., Senthil Kumar, P., Saravanan, A., Ravikumar, C., Jaikumar, V., 2017. Prediction and interpretation of adsorption parameters for the sequestration of methylene blue dye from aqueous solution using microwave assisted corncob activated carbon. Sustainable Materials and Technologies 11, 1–11. https://doi.org/10.1016/j.susmat.2016.11.001.
Tran, H.V., Bui, L.T., Dinh, T.T., Le, D.H., Huynh, C.D., Trinh, A.X., 2017. Graphene oxide/Fe3O4/chitosan nanocomposite: a recoverable and recyclable adsorbent for organic dyes removal. Application to methylene blue. Mater. Res. Express 4 (3), 035701. https://doi.org/10.1088/2053-1591/aa6096.
Tran, H.V., Hoang, L.T., Huynh, C.D., 2020. An investigation on kinetic and thermodynamic parameters of methylene blue adsorption onto graphene-based nanocomposite. Chem. Phys. 535, 110793. https://doi.org/10.1016/j.chemphys.2020.110793.
Wang, S., Zhu, Z.H., Coomes, A., Haghseresht, F., Lu, G.Q., 2005. The physical and surface chemical characteristics of activated carbons and the adsorption of methylene blue from wastewater. J. Colloid Interface Sci. 284, 440–446. https://doi.org/10.1016/j.jcis.2004.10.050.
Wang, X., Liu, B., Lu, Q., Qu, Q., 2014. Graphene-based materials: fabrication and application for adsorption in analytical chemistry. J. Chromatogr. A 1362, 1–15. https://doi.org/10.1016/j.chroma.2014.08.023.
Wang, Z., Han, Q., Xia, J., Xia, L., Ding, M., Tang, J., 2013. Graphene-based solid-phase extraction disk for fast separation and preconcentration of trace polycyclic aromatic hydrocarbons from environmental water samples. J. Separ. Sci. 36, 1834–1842. https://doi.org/10.1002/jssc.201300186.
Wang, Z., Gao, M., Li, X., Ning, J., Zhou, Z., Li, G., 2020. Efficient adsorption of methylene blue from aqueous solution by graphene oxide modified persimmon tannins. Mater. Sci. Eng. C 108, 110196. https://doi.org/10.1016/j.msec.2019.110196.
Xing, M., Xu, L., Wang, J., 2016. Mechanism of Co(II) adsorption by zero valent iron/graphene nanocomposite. J. Hazard Mater. 301, 286–296. https://doi.org/10.1016/j.jhazmat.2015.09.004.
Yang, S., Chen, S., Chang, Y., Cao, A., Liu, Y., Wang, H., 2011. Removal of methylene blue from aqueous solution by graphene oxide. J. Colloid Interface Sci. 359, 24–29. https://doi.org/10.1016/j.jcis.2011.02.064.
Yang, S.T., Chang, Y., Wang, H., Liu, G., Chen, S., Wang, Y., Liu, Y., Cao, A., 2010. Folding/aggregation of graphene oxide and its application in Cu2+ removal. J. Colloid Interface Sci. 351, 122–127. https://doi.org/10.1016/j.jcis.2010.07.042.
Yao, Y., Xu, F., Chen, M., Xu, Z., Zhu, Z., 2010. Adsorption behavior of methylene blue on carbon nanotubes. Bioresour. Technol. 101, 3040–3046. https://doi.org/10.1016/j.biortech.2009.12.042.
Zhang, W., Zhou, C., Zhou, W., Lei, A., Zhang, Q., Wan, Q., Zou, B., 2011. Fast and considerable adsorption of methylene blue dye onto graphene oxide. https://doi.org/10.1007/s00128-011-0304-1, 87, 86, 90.
Zhao, M., Tang, Z., Liu, P., 2008. Removal of methylene blue from aqueous solution with silica nano-sheets derived from vermiculite. J. Hazard Mater. 158, 43–51. https://doi.org/10.1016/j.jhazmat.2008.01.031.